Journal of Sound and Vibration 553 (2023) 117675

Contents lists available at ScienceDirect

Journal of Sound and Vibration

journal homepage: www.elsevier.com/locate/jsvi

Equivalent oscillator approach to model vortex induced vibrations on a circular cylinder

T. Argentini, S. Muggiasca *, G. Notaro, D. Rocchi, F. Zanelli

Department of Mechanical Engineering, Politecnico di Milano, Via La Masa 1, 20156, Milan, Italy

ARTICLE INFO

Keywords:
Vortex induced vibration
Circular cylinder
Equivalent oscillator
Parameters identification
Genetic algorithm
Wind tunnel test

ABSTRACT

The paper presents a numerical model, based on the equivalent oscillator approach, able to simulate vortex induced vibrations on a circular cylinder. This model consists of a single degree of freedom mechanical system characterized by non-linear parameters that reproduce the fluid-structure interaction in time domain. A genetic algorithm approach was used in order to identify the characteristic parameters of the equivalent oscillator: obtained results are discussed and compared with wind tunnel experimental data and with a previous version of the numerical model. Comparison is performed both in terms of aerodynamic forces and oscillation amplitudes and both in steady and transient conditions.

1. Introduction

The flow around an oscillating cylinder was deeply investigated in past years, especially by means of experimental tests. In particular, Sarpkaya [1], Williamson and Govardhan [2] and Bearman [3] studied in detail this topic, giving a complete overview of Vortex Induced Vibration (VIV) phenomenon for a circular cylinder. Several researches studied different aspects of the physical problem: cylinders in forced motion conditions [4], rigid circular cylinders elastically mounted and free to vibrate [5] and flexible cylinders [6]. All these past research studies described the main features of VIV on circular cylinders highlighting the complexity of the phenomenon: despite the simplicity of the structure dynamics, the wind-structure interaction is very complex with a strong dependence on several parameters as Reynolds number, structural damping ζ_s and mass ratio m^*.

As reported in previous researches, the steady-state response of a circular cylinder subjected to vortex shedding is characterized by the presence of a synchronization range called the "lock-in" region of reduced velocity $U^* = U/(f_n D)$: outside this region vortices are typically detaching according to the Strouhal law ($f = StU/D$) and the shedding frequency is directly proportional to the flow velocity. Within the lock-in region, vortex shedding frequency is synchronized with the natural frequency of the body and Strouhal law is no more respected. Moreover, the response amplitude has different characteristics as a function of the reduced velocity: in particular three different branches can be recognized, "initial", "upper" and "lower" branches. At the Strouhal velocity U_{St}, vibration amplitudes start increasing along the so-called "initial branch" [2,7], while vortices are detaching according to the body natural frequency, regardless of the flow velocity. Increasing the wind speed, a change in the slope of the curve is highlighted, showing the beginning of the "upper branch" [2,7]. In this branch, the fluid-structure interaction leads the cylinder to reach large amplitudes of vibration, which are synchronized with the detaching vortices. At a certain velocity, the flow and the body are no more synchronized, and vibrations suddenly decrease. These three branches are characterized by different types of vortexes as stated in Williamson and Roshko [4] where

* Corresponding author.
E-mail address: sara.muggiasca@polimi.it (S. Muggiasca).

https://doi.org/10.1016/j.jsv.2023.117675
Received 23 August 2022; Received in revised form 10 March 2023; Accepted 13 March 2023
Available online 15 March 2023

Nomenclature

m_L	Linear mass
m^*	Mass ratio, $\frac{m_L}{\pi\rho D^2/4}$
U	Incoming wind speed
ρ	Air density
St	Strouhal Number
f	Vortex shedding frequency
ω	Vortex shedding circular frequency
f_n	Natural frequency
ω_n	Natural circular frequency
ζ_s	Structural non-dimensional damping
D	Cylinder diameter
L	Cylinder length
U_{St}	Strouhal velocity, $\frac{f_n D}{St}$
F_L	Lift force
C_L	Lift coefficient, $F_L/(0.5\rho U^2 LD)$
Sc	Scruton Number, $Sc = \frac{2\pi m_L \zeta_S}{\rho D^2}$
Re	Reynolds Number, $Re = \frac{\rho DU}{\mu}$
μ	air dynamic viscosity
x	Cylinder vertical displacement

a map of vortex patterns is presented.

Several experimental campaigns have been carried out in the Politecnico di Milano wind tunnel in order to study more in detail the VIV mechanisms with particular attention to high mass ratio (m^*) and high Reynolds Numbers conditions: considering civil engineering applications that involve circular-shaped structures, high Re and high mass ratio are the typical experienced conditions. During the tests, particular care was devoted to studying the power input mechanisms in the different branches, both for steady-state and for the transient evolution of the oscillating amplitudes at constant wind speed. As highlighted in Zasso et al. [7], Belloli et al. [8], Muggiasca et al. [9], the relative phase between aerodynamic force and cylinder displacement plays a key role in the energy input definition: during the performed experimental campaign a 'phase effective' mechanism was observed at small oscillation amplitudes when the relative phase is close to 90°, while, when amplitudes increase, the power input was limited by the phase that tends to zero.

In order to increase the capability to predict cylinders behavior in different flow conditions, several numerical models have been developed in the last years to reproduce the main features of the fluid-structure interaction of circular cylinders. In particular, it can be distinguished between models aimed at representing the complete fluid dynamics of vortex induced vibrations, and models aimed at reproducing the structural response of this phenomenon. A full reproduction of the vortex induced vibrations is obtained through CFD models, which are used to compute an approximated solution of the Navier-Stokes equations, under specific boundary conditions. The application of CFD techniques permit to obtain good results for rigid structure at relative low Reynold numbers (see Navrose and Mittal [10], but the numerical treatment of turbulent and high Reynold number flows is still complex and computationally expensive. Studies concerning applications at high Re are improving the quality of their results, as in Mandelli et al. [11] and Mandelli et al. [12] that present a good numerical reproduction of the experimental data measured in the Politecnico di Milano wind tunnel for Re up to 5 10^4. Nevertheless, this approach cannot be easily generalized and requires big computational efforts for engineering applications characterized by not only high Reynolds numbers but also a strong interaction between structural flexibility and global aerodynamic behavior.

Hence some alternative ways to compute VIV without solving the Navier-Stokes equations have been investigated. From this point of view, a simplified approach is presented in the Eurocode [13], where some criteria for evaluating the vortex shedding impact on the specific design case are given. In particular, according to section E.1.5, the design amplitude of vibration is computed following some straightforward methods. This approach focuses more on the vortex shedding effects on the structure rather than the physical phenomenon itself. The Eurocode approach is effective to give an estimation for certain design procedures, but it doesn't consider the physics of the phenomenon: it is not able to reproduce the different branches of the dynamic response at different reduced velocity ranges.

Another possible approach is represented by phenomenological models based on wake oscillators [14–17]: these models try to simulate the physical nature of VIV developing a non-linear model for aerodynamic forces, to be coupled with the 1 dof system of the structure. They can reproduce the main features of the VIV reducing the computational costs compared to CFD, in particular their integration with FEM models is profitable in evaluating aerodynamic behavior in flexible civil structures. In Facchinetti et al. [18] the basic van der Pol kernel is considered, analyzing different coupling terms for the fluid-structure interactions: the presented results highlighted a good qualitative agreement with experimental literature data with quantitative matches for some VIV issues. Further improvements of the model are proposed in Ogink and Metrikine [19]: the authors modified the model parameters by introducing a dependence on the frequency to simulate both forced and free vibration experiments and to better describe the cylinder behavior in the

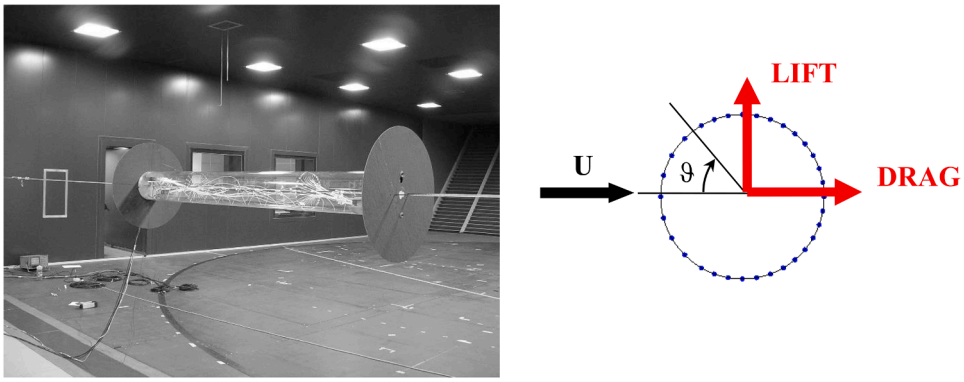

Fig. 1. Rigid cylinder model installed in the Politecnico di Milano Wind Tunnel (a) Pressure taps set-up (b).

different branches. Manish et al. [20] used the same formulation to reproduce the cylinder behavior in both cross-wind and inline directions. These researches lead to an improvement in the model formulation even if differences with respect to reference experimental data are still valuable.

The oscillator model proposed in the present paper, the 'equivalent oscillator model', develops a mechanical structure similar to the one proposed by Hartlen and Currie [15], modeling the aerodynamic lift force as a non-linear function of the cylinder oscillation amplitude. This model reproduces the components in phase and in quadrature of the aerodynamic force field, in terms of equivalent rheological elements able to simulate the interaction between flow and structure as a function of the system state and the flow conditions. The flow field is defined by equivalent mass, stiffness and damping parameters able to modify the structural characteristics of the cylinder: this keeps the aerodynamic forces formulation related to the aeroelastic behavior of the structure. The key point in the model definition concerns the tuning of the characteristic parameters and the implementation of the non-linear functions used to define the aerodynamic forces. In particular, taking advantage of the experimental tests performed in the Politecnico di Milano wind tunnel, the tuning process was developed considering not only the maximum response experienced by the structure in the lock-in region, but also other issues considered important for civil applications as:

- The structure behavior in transient conditions
- The proper reproduction of the aerodynamic lift force and its relative phase relating to the displacement
- The dimension of the lock-in region and the structure behavior outside this region
- The effect of the structural flexibility and the VIV development along the structure

Previous works, developed by Politecnico research group, used a polynomial formulation to simulate VIV non-linearities [21,22]: the potentiality of this approach was demonstrated in reproducing the whole structural behavior of civil applications as in Argentini et al. [23] and Belloli et al. [24] where a series of equivalent oscillators have been attached to a FE model of a cable-stayed bridge under construction. Recently the equivalent oscillator was satisfactorily applied to reproduce the behavior of cylindrical legs of a high observation wheel supporting frame: numerical results were used to design the TMD damping system to control VIV [25]. This formulation was able to properly reproduce the maximum amplitudes reached in the lock-in region, but it was not so accurate in describing the three branches, especially in terms of lift force. Moreover, the control of the steady-state condition after the transient needed to be improved. For this reason, further studies were developed in order to find new non-linear formulations and key parameters able to improve the performance of the numerical model. The idea is to obtain a model for civil applications (high Reynolds Numbers, free motion in air) applicable to like-cylindrical shape structure. The present work aims to present the preliminary results obtained in the new developments of the model with particular reference to the process to identify its characteristic parameters. Genetic algorithm approach was used for the identification: the genetic algorithm functions are implemented in MATLAB using a subset of the Evolutionary Algorithms [26]. These methods are used to solve non-linear problems of parameters identification: the procedure consists of setting up an initial population of the parameters, which are selected throughout the generations according to their performances on a best-fitting function minimization. The idea relies on the "survival of the fittest" Darwinian concept [26], by which the best parameters have a higher probability to be passed to the next generations [27]. In the genetic algorithm are also implemented features as crossover and mutation, accounting for the randomness of the natural selection process. The experimental database considered for identification and validation is represented by the data collected during the last years in several tests campaigns performed in Politecnico di Milano Boundary Layer Wind Tunnel. A rigid circular cylinder suspended on springs and free to vibrate in the crossflow direction has been tested measuring the amplitude of vibration and the aerodynamic forces [7–9,28,29]. Data collected in steady-state conditions have been used for the identification while the ones obtained in transient conditions have been used for the preliminary validation. The model results collected in the present paper represent a first step for future validation to be performed on sets of data obtained with different models tested in different conditions.

Table 1
Main model and set-up characteristics.

Diameter (m)	0.2
Length (m)	2
Linear mass (kg/m)	6.5
Aspect ratio L/D	10
Natural frequency (Hz)	3.1
Mass ratio	177
Strouhal Number	0.18
Strouhal velocity (m/s)	3.37
Reynolds Number (nominal value in lock-in region)	$5{\cdot}10^4$
Non-dimensional damping range	$0.5\ 10^{-3}$ – $1.5\ 10^{-3}$
Scruton Number range	0.42 – 1.27

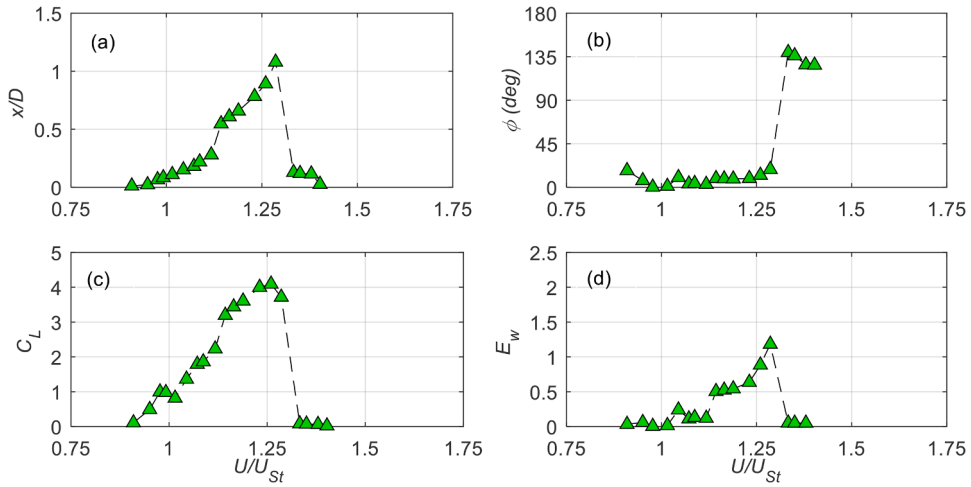

Fig. 2. Steady-state response of the oscillating cylinder in the lock-in region: (a) non-dimensional oscillation amplitude, (b) relative phase, (c) lift coefficient, (d) non-dimensional power input.

The paper is structured into four main sections, in the first one the experimental database is presented, then the numerical model is described, the identification procedure is introduced and finally, the main results and conclusions are discussed.

2. Experimental setup and results

Several experimental campaigns on a rigid circular cylinder, elastically suspended and free to oscillate in the cross-flow direction, were performed at Politecnico di Milano Wind Tunnel (see Fig. 1(a)). The very large test section (14 × 4m) allows for negligible blockage effects (0.7%) in smooth flow conditions ($I_u \cong 2\%$). The model was suspended through tensioned cables in order to separate horizontal, torsional and vertical natural frequencies allowing to study the vortex induced oscillations of the cylinder in cross-wind direction. The main characteristics of the model and the set-up are summarized in Table 1. It is possible to note that the tested model is characterized by high Reynolds Number and high mass ratio values, typical of civil applications.

The model was instrumented through a high-frequency pressure scanner (sampling rate up to 125 Hz), installed inside the model to map the instantaneous pressure field on 32 pressure taps (see Fig. 1(b)). The pressure measurements were performed along one section of the rigid cylinder that is considered representative of the pressure distribution along the rigid model due to its aspect ratio equal to 10. The dynamic response of the cylinder was measured by means of two vertical accelerometers while a horizontal one checks possible in-line motions. Accelerometers accuracy in defining the cylinder motion was directly verified by measuring the displacement also through a laser. Aerodynamic forces were obtained by integrating pressure signals on the instrumented section (conventions are reported in Fig. 1(b)). Pressure data and accelerations were fully synchronized in order to have a simultaneous evaluation of forces and motion. The used set-up permitted to properly define, not only the cylinder response under vortex shedding excitation, but also the pressure field around the cylinder surface during the motion and the evolution of aerodynamic forces. A more detailed description of the wind tunnel set-up and of the model characteristics are reported in Belloli et al. [29] and Muggiasca et al. [9].

During the experimental campaign three kinds of tests were performed in smooth flow conditions:

- Build-up tests: the cylinder is released from rest at a fixed wind velocity, in lock-in range, and the vibration amplitude variation is monitored (the amplitude increases until a limit cycle is reached);

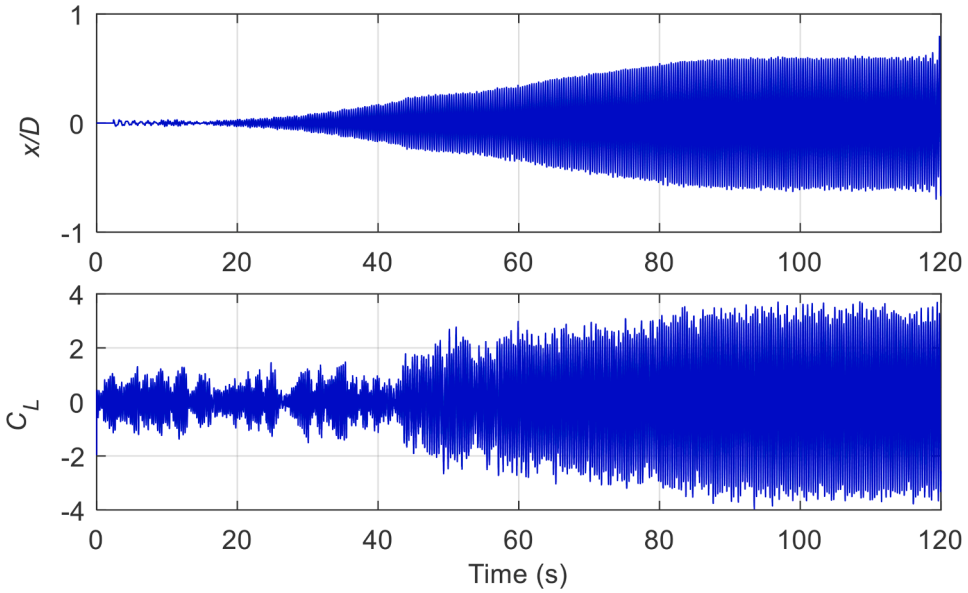

Fig. 3. Build-up time history at $\mathbf{U}/\mathbf{U_{St}} = 1.17$: non-dimensional amplitude (a) and lift coefficient (b) as a function of time.

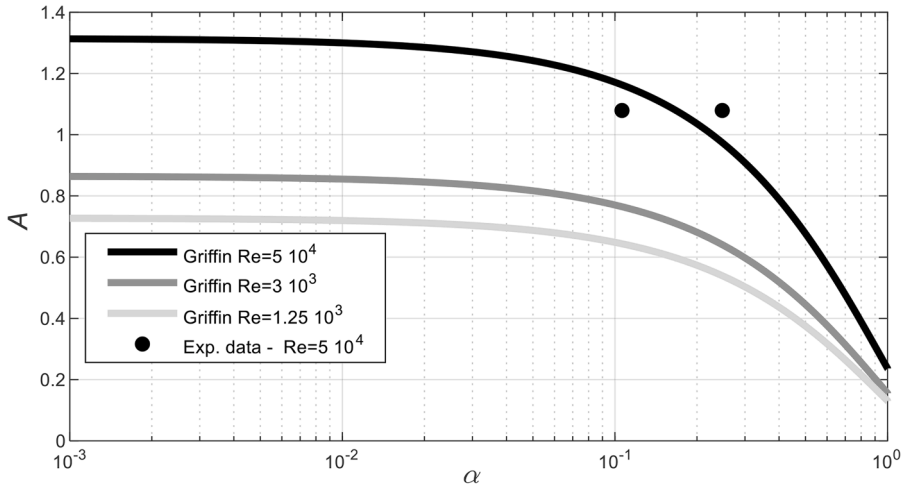

Fig. 4. 'Modified Griffin plot' ([31]): literature data compared with experimental data measured in the Politecnico di Milano wind tunnel (A^* is the cylinder maximum non-dimensional oscillation amplitude and $\boldsymbol{\alpha}$ is the mass-damping parameter $m^*\zeta$).

- Decay tests: initial conditions have been imposed to the cylinder with motion amplitude larger than the corresponding steady-state value at fixed wind speed, then the vibration amplitude variation is measured (the amplitude decreases until the steady-state condition is reached). These tests were performed outside of the lock-in region and inside the region for the low-amplitudes points;
- Progressive regime tests: steady-state conditions at fixed wind speed are acquired. The wind velocity is changed by small steps, waiting for the new steady-state condition achievement before recording.

Moreover, decay tests in still air were performed to evaluate the structural characteristics of the model: the main structural parameters (natural frequency and non-dimensional damping) are summarized in Table 1.

Fig. 2 reports the steady-state results in terms of normalized oscillation amplitudes x/D, lift force coefficient defined as $C_L = F_L/0.5\rho U^2 DL$, relative phase between force and displacement ϕ, non-dimensional power input E_w: all the quantities are shown as a function of the non-dimensional velocity U/U_{St}.

The oscillation amplitude x has been obtained via double integration of the accelerometer signals, considering the peak of the displacement spectrum at the cylinder natural frequency. The lift coefficient represents the force component synchronized with the cylinder displacement, i.e. the locked-in vortex shedding force. The phase ϕ is the phase of the locked-in force component with respect

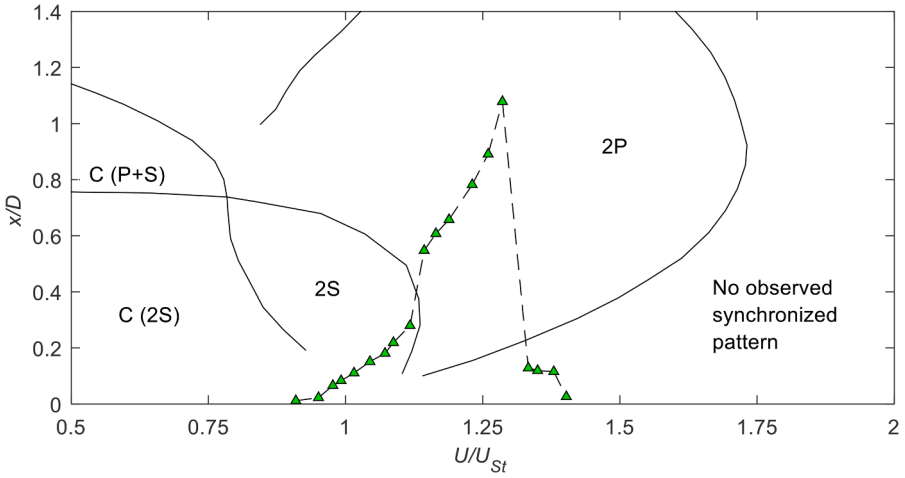

Fig. 5. Steady-state oscillating displacement and vortex modes ([4]).

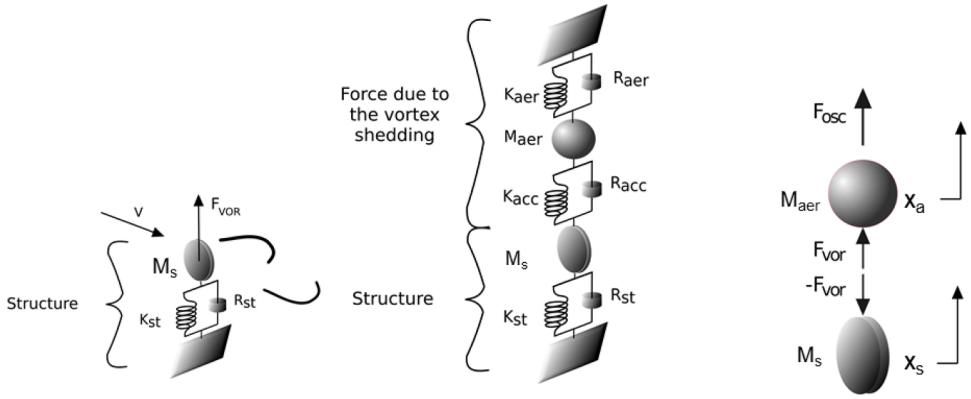

Fig. 6. The Equivalent Oscillator.

to the cylinder. The non-dimensional energy input is calculated as in Eq. (1) and reported in Fig. 2 as well.

$$E_w = \frac{E}{\pi q D L x} = C_L \sin(\phi) \tag{1}$$

An example of results in transient conditions is the build-up time history reported in Fig. 3.

As highlighted in Belloli et al. [8], the experimental results measured at the Politecnico di Milano wind tunnel represent a database characterized by high *Re* and high mass ratio values: this permitted to experience very peculiar conditions few represented in literature. However, the measured data are in line with the 'modified Griffin plot' reported in Fig. 4 where both *Re* and m^* are considered in predicting the oscillation amplitudes. Despite the high mass ratio, high oscillation amplitudes are reached and these can be related to the typical upper branch conditions as the representation of the steady-state response curve in the map of vortex patterns suggested (see Fig. 5).

A complete presentation of the experimental results has been reported in Zasso et al. [7], Belloli et al. [8], Muggiasca et al. [9], Zasso et al. [28], Belloli et al. [29].

3. Equivalent oscillator model

The Equivalent Oscillator Model used in this research is a mechanical model developed to reproduce the forcing due to the vortex shedding on a bluff body i.e. a circular cylinder. This takes inspiration from the Hartlen and Currie model [15], representing the aerodynamic forces in terms of equivalent elastic and damping elements. The main structure of the model was previously developed by the Politecnico di Milano research group [21,22], and the present paper presented its last version obtained properly defining the characteristics parameters and the non-linear functions.

The body is modeled as 1 dof elastically suspended circular cylinder; constrained to oscillate transversely in a uniform flow (see Fig. 6). The structure is represented by its modal parameters in terms of mass, M_s, stiffness, K_s, and damping, R_s. The equation of

Table 2
Equivalent Oscillator Parameters.

$= qDL\ H_{\mathrm{kaer}}\frac{1}{D}$	$K''_{\mathrm{aer}} = qDL\ K_{\mathrm{kaer}}\frac{1}{D}$
$R'_{\mathrm{aer}} = qDL\ H_{\mathrm{raer}}\frac{1}{\omega D}$	$R''_{\mathrm{aer}} = qDL\ K_{\mathrm{raer}}\frac{1}{\omega D}$
$K'_{\mathrm{acc}} = qDL\ H_{\mathrm{kacc}}\frac{1}{D}$	$K''_{\mathrm{acc}} = qDL\ K_{\mathrm{kacc}}\frac{1}{D}$
$R'_{\mathrm{acc}} = qDL\ H_{\mathrm{racc}}\frac{1}{\omega D}$	$R''_{\mathrm{acc}} = qDL\ K_{\mathrm{racc}}\frac{1}{\omega D}$

motion of this simple vibrating system is reported in Eq. (2) where x_s is the cylinder displacement in vertical direction and F_{aero} is the aerodynamic force due to VIV.

$$M_s\ddot{x}_s + R_s\dot{x}_s + K_s x_s = F_{\mathrm{aero}} \tag{2}$$

From the experiments, it was observed that this aerodynamic force is a function of the vibration amplitudes both in phase and in quadrature: these components can be modeled by equivalent springs and dampers that coupled the wake model to the structural one. The wake model consists of a non-linear one degree of freedom oscillator, made up of a mass, M_{aer}, connected to the cylinder and to the ground through springs and dampers characterized by parameters that are a function of the cylinder state. In Fig. 6, R_{aer} and K_{aer} represent the connections elements between the aerodynamic mass and the ground, while R_{acc} and K_{acc} connected the flow mass and the structure resulting in the coupling terms. The mass ideally represents the flow that moves together with the structure, while the connection elements try to reproduce the interaction between the structure itself and the flow field.

The complete model reported in Fig. 6 (wake model + structure) results in a two degree of freedom system, where x_a is the degree of freedom of the aerodynamic mass and x_s the cylinder's one and its equations of motion are reported in Eq. (3):

$$\begin{aligned} M_s\ddot{x}_s + R_s\dot{x}_s + K_s x_s &= -F_{\mathrm{vor}}(x_a,\ \dot{x}_a, x_s,\ \dot{x}_s, U) \\ M_{\mathrm{aer}}\ddot{x}_a &= F_{\mathrm{vor}}(x_a,\ \dot{x}_a, x_s,\ \dot{x}_s, U) - F_{\mathrm{osc}}(x_a,\ \dot{x}_a, U) \end{aligned} \tag{3}$$

where U is the incoming wind velocity, F_{vor} is the coupling force and F_{osc} is the force due to the damper and the spring that constrain the oscillator to the ground.

In order to properly reproduce the force field non-linearities, each connection element is modeled as reported in Eq. (4) with a linear and a non-linear component.

$$\begin{aligned} K_{\mathrm{acc}} &= K'_{\mathrm{acc}} + K''_{\mathrm{acc}} f_1(x_s - x_a) \\ R_{\mathrm{acc}} &= R'_{\mathrm{acc}} + R''_{\mathrm{acc}} f_2(\dot{x}_s - \dot{x}_a) \\ K_{\mathrm{aer}} &= K'_{\mathrm{aer}} + K''_{\mathrm{aer}} f_3(x_a) \\ R_{\mathrm{aer}} &= R'_{\mathrm{aer}} + R''_{\mathrm{aer}} f_4(\dot{x}_a) \end{aligned} \tag{4}$$

where f_1, f_2, f_3 and f_4 are non-linear functions of the system degrees of freedom combinations and their derivatives. The coefficients included in the previous equations are expressed as a function of the incoming wind velocity, the fluid density, the cylinder dimensions and the vortex shedding circular frequency for the damping terms (see Table 2 where $q = 1/2\rho U^2$ is the dynamic pressure of the incoming flow and $\omega = 2\pi \cdot \mathrm{StU/D}$).

Substituting the forces formulation in (3) we obtain (Eq. (5)):

$$\begin{aligned} F_{\mathrm{vor}}(x_a,\ \dot{x}_a, x_s,\ \dot{x}_s, U) &= -[K'_{\mathrm{acc}} + K''_{\mathrm{acc}} f_1(x_s - x_a)](x_s - x_a) - [R'_{\mathrm{acc}} + R''_{\mathrm{acc}} f_2(\dot{x}_s - \dot{x}_a)](\dot{x}_s - \dot{x}_a) \\ F_{\mathrm{osc}}(x_a,\ \dot{x}_a, U) &= -[K'_{\mathrm{aer}} + K''_{\mathrm{aer}} f_3(x_a)]x_a - [R'_{\mathrm{aer}} + R''_{\mathrm{aer}} f_4(\dot{x}_a)]\dot{x}_a \end{aligned} \tag{5}$$

The capability of the model to simulate VIV phenomenon is strictly related to a proper definition of the characteristic constant and dimensionless parameters reported in Table 2 (H_{kaer}, H_{raer}, H_{kacc}, H_{racc}, K_{kaer}, K_{raer}, K_{kacc}, K_{racc}) and of the formulation of the functions f_1, f_2, f_3 and f_4, included in Eq. (4). For this reason, the identification procedure is an important key point, discussed in the following section. In the identification process, the relation between the aerodynamic mass M_{aer} and the linear stiffness parameters K'_{aer} and K'_{acc} must be taken in consideration as in Eq. (6):

$$\omega_{St} = \sqrt{\frac{K'_{\mathrm{aer}} + K'_{\mathrm{acc}}}{M_{\mathrm{aer}}}} \tag{6}$$

This is to grant that, when the cylinder is at rest, the oscillator vibrates accordingly to the Strouhal frequency associated with the current flow velocity; in this condition, the Strouhal frequency will be properly reproduced also in the lift force.

Moreover, to obtain a negative damping ratio of the whole system, i.e. to reproduce the energy introduced in lock-in region, an eigenvalue of the two d.o.f. system must have a positive real part. This feature can be achieved by imposing a negative damping coefficient to the aerodynamic mass damper (R_{aer}).

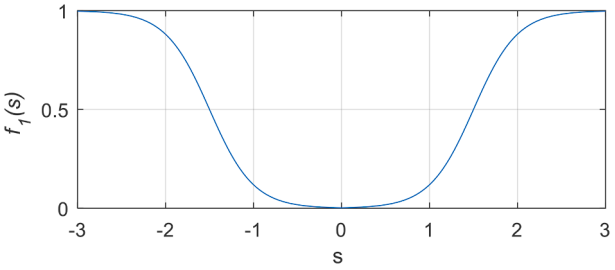

Fig. 7. Non-linear function $f_1(s)$.

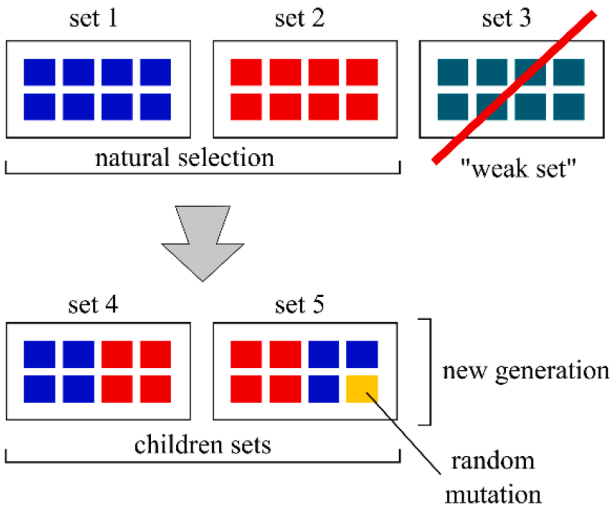

Fig. 8. Sketch of the Genetic algorithm process.

4. Model parameters definition

The main parameters of the equivalent oscillator (see Table 2) and the functions introduced in Eq. (4) are identified from experimental data using genetic algorithm based approach.

In particular, for the identification, the steady-state response was used, while the transient tests (Decay and build-up tests) were used for the validation. Steady-state response curves were selected for the identification, as these were considered more suitable, summarizing the VIV main features.

Both forces and displacements were considered a mandatory target to properly model the VIV behavior, as the correct reproduction of the energy input mechanism is considered crucial in fluid-structure interaction for civil applications. Only free responses have been evaluated, while forced vibrations were not considered, as out of the scope of the research. In previous work ([22]) a polynomial formulation was proposed to reproduce the VIV non-linearities, further analysis highlighted that functions based on hyperbolic tangents functions are more suitable to limit their effect only in the lock-in region and to control the maximum reached oscillation amplitudes.

An example of the functions behaviour is shown in Fig. 7 varying the generic argument 's', the generic expression for the four functions is reported in Eq. (7). .

$$\begin{aligned} f_1(x) &= a_1[b_1 + \tanh(c_1(\mathrm{abs}(s) - d_1))] \quad s = x_s - x_a \\ f_2(x) &= a_2[b_2 + \tanh(c_2(\mathrm{abs}(s) - d_2))] \quad s = \dot{x}_s - \dot{x}_a \\ f_3(x) &= a_3[b_3 + \tanh(c_3(\mathrm{abs}(s) - d_3))] \quad s = x_a \\ f_4(x) &= a_4[b_4 + \tanh(c_4(\mathrm{abs}(s) - d_4))] \quad s = \dot{x}_a \end{aligned} \tag{7}$$

Each function is characterized by four parameters to be identified, leading to, together with the eight included in Table 2, a total number of parameters equal to twenty-four. As a starting point for the identification procedure, the parameters of a previous version of the model were considered: in this version, the non-linearities were represented similarly but the used parameters were not optimized.

The procedure was developed using both MATLAB and FORTRAN codes. Firstly the initial population and the limits of variation of the twenty-four parameters were set and then the Genetic Algorithm (see sketch reported in Fig. 8) was launched.

The obtained set of parameters is analyzed returning a value, based on the evaluation of the numerical error with respect to the experimental data: the smaller the error the higher is the probability of these parameters to be called in the future. Reaching the fixed

Table 3
Equivalent oscillator parameters obtained from the optimization procedure.

a_1	b_1	c_1	d_1	a_2	b_2	c_2	d_2
1.002	1.050	1.599	1.439	1.089	1.332	2.023	1.630
a_3	b_3	c_3	d_3	a_4	b_4	c_4	d_4
4.252	0.911	1.105	2.498	1.000	0.999	1.752	1.947
$\boldsymbol{H}_{\mathbf{kacc}}$	H_{racc}	H_{kaer}	H_{raer}	K_{kacc}	K_{racc}	K_{kaer}	K_{raer}
1.300	0.949	2.376	-0.878	1.451	12.345	-0.762	-0.250

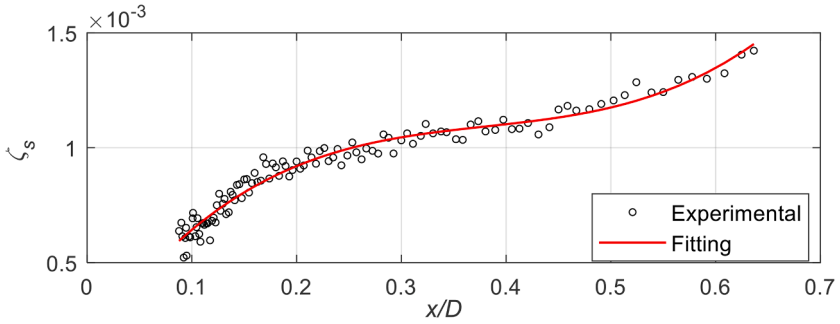

Fig. 9. Structural non-dimensional damping as a function of the oscillation amplitude.

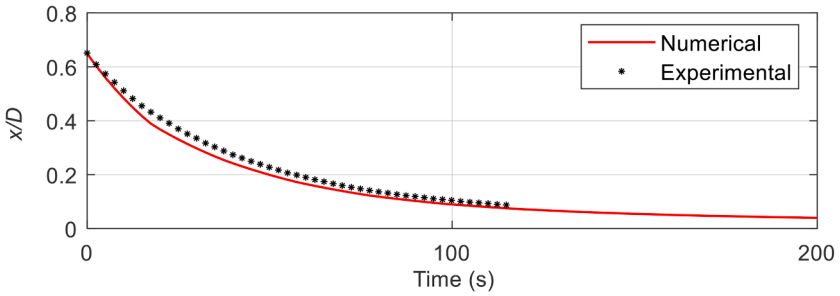

Fig. 10. Decay tests in still air.

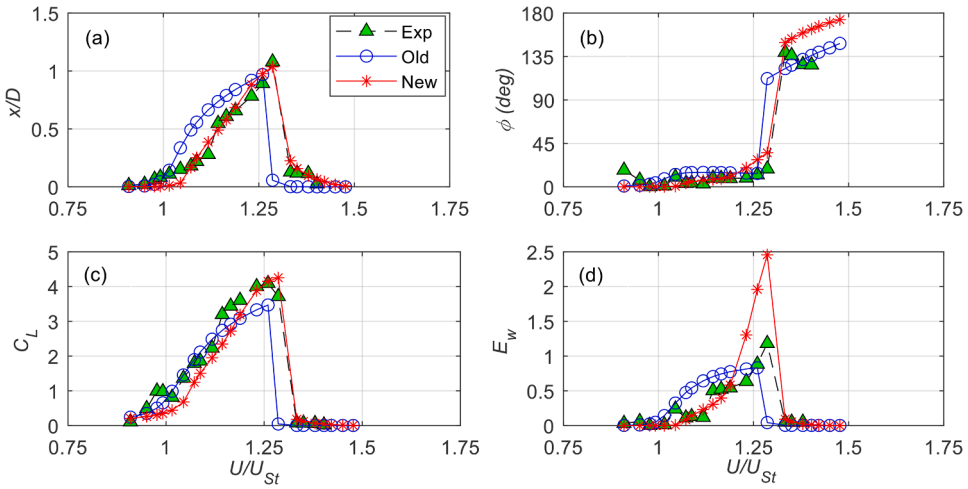

Fig. 11. Steady-state response of the oscillating cylinder in the lock-in region: (a) non-dimensional oscillation amplitude, (b) relative phase, (c) lift coefficient, (d) non-dimensional power input. Comparison between numerical (old and new) and experimental results.

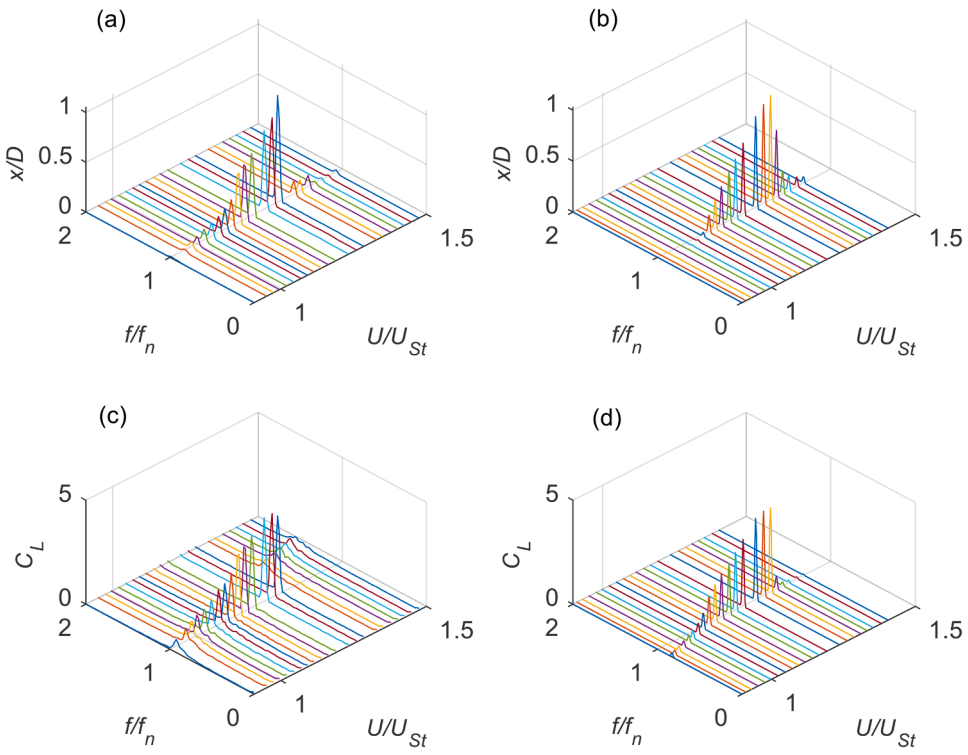

Fig. 12. Non-dimensional displacement ((a) Experimental, (b) Numerical - New) and lift force coefficient ((c) Experimental, (d) Numerical – New) spectra, for the steady-state points, as a function of the normalized frequency and of the velocity ratio.

tolerance or the maximum number of "generations", the algorithm stops and returns the best-evaluated set. The error used as a target of the identification procedure was evaluated considering oscillation amplitude, the lift force and phase values in steady-state conditions. Several campaigns have been carried out to refine the parameters and the best obtained configuration is reported in Table 3.

The comparison between numerical simulations and experimental results is reported in section 5.

4.1. Variable structural damping

In the proposed formulation the dependence of the structural damping ratio to the vibration amplitude has been included in the model.

The curve reported in Fig. 9, describing the relationship between the structural non-dimensional damping factor and the non-dimensional oscillation amplitude, was approximated through a 3rd order polynomial function and it was inserted in the code, to compute, at each time step, the actual structural damping ratio. The implementation has been successfully tested in no-wind numerical simulations, in which the code was able to reproduce the physical behavior of the cylinder (see Fig. 10 where the decay oscillation amplitude decrease is reported in terms of envelope of the maximum oscillation amplitudes).

5. Results and discussion

In this section, the main results of the numerical model simulations are reported. Fig. 11 shows the new numerical steady-state response curves (red curves), compared with the experimental data. The numerical results of the old model (blue curves) are included as well, representing the starting point before the optimized identification. It is possible to note that with the new parameters, the experimental curves are more accurately reproduced both in maximum values and trends. There is only an overestimation of the peak of the non-dimensional power input deriving from a slight overestimation of the phase before the "jump".

The good reproduction of the steady-state conditions was expected as the steady-state data were used as database for the identification procedure. In particular, the results are good in the upper branch for oscillation amplitudes and lift force and also the width of the lock-in region is properly reproduced. The separation between initial and upper branch is not so evident, while is remarkable the jump toward lower branch.

The comparison between the new model results and the experimental data has been considered also in terms of harmonic content. In Fig. 12 the spectra of non-dimensional oscillation amplitude and the lift coefficient are reported for the different wind velocities within the lock-in region: it is possible to note that both for the experimental data and the numerical ones, the signals are mainly monoharmonic especially as far it concerns the displacement. The lift coefficient experienced broadband spectra around the main

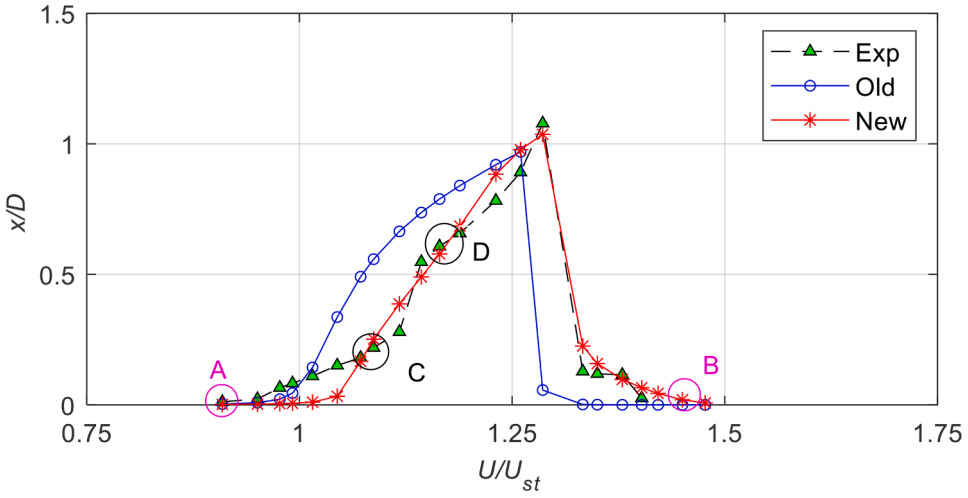

Fig. 13. Transient tests conditions represented on the steady-state curves.

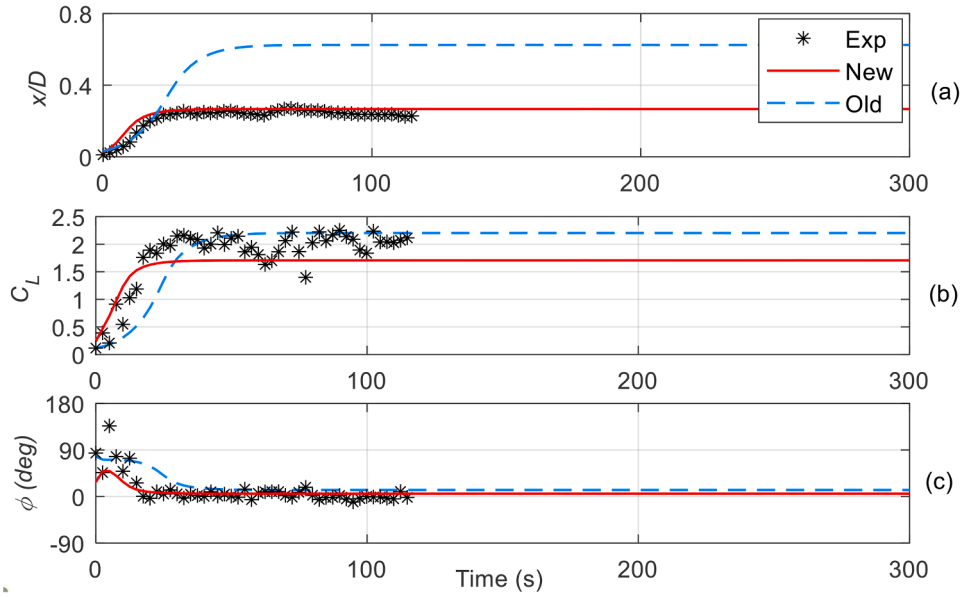

Fig. 14. Build-up test, numerical-experimental comparison: point C in Fig. 13 ($\boldsymbol{U} = 3.7\ \mathbf{m/s}$, $\boldsymbol{U/U_{St}} = 1.09$): (a) non-dimensional oscillation amplitude, (b) lift coefficient, (c) relative phase.

frequency at the extremities of the look-in region, larger in the experimental case: in these extremity cases, it is possible to note that the main frequency follows the Strouhal law as the phenomenon is not yet synchronized.

The performance of the new numerical model was then evaluated in terms of transient response: two build-up curves (point C in the initial branch and point D in upper branch) and two wind decay curves (point A before and point B after lock-in range) where considered, as shown in Fig. 13. Lower branch was not considered as, in this part of the lock-in region, transients are generally longer and less relevant for civil applications. The transient curves have been obtained considering the harmonic components of the lift force and the cylinder oscillation amplitude at the cylinder's natural frequency, evaluated over about 10 cycles, using for the analysis a moving window with an overlap of 50%. This procedure is particularly useful for experimental data analysis, to separate the effects of the two frequencies present in lift coefficient when the synchronization of the phenomenon is not fully happened,

In Fig. 14 and in Fig. 15, the new model is compared with the experimental data and with the old ones: it is possible to note that the new model is able to fit quite well the transient time histories proposed, in terms of displacement, force and phase and both considering the regime values and the transient duration.

Also for points A and B, the decays outside the lock-in range, the new model represents an improvement in reproducing the oscillation amplitudes trend (see Figs. 16 and 17).

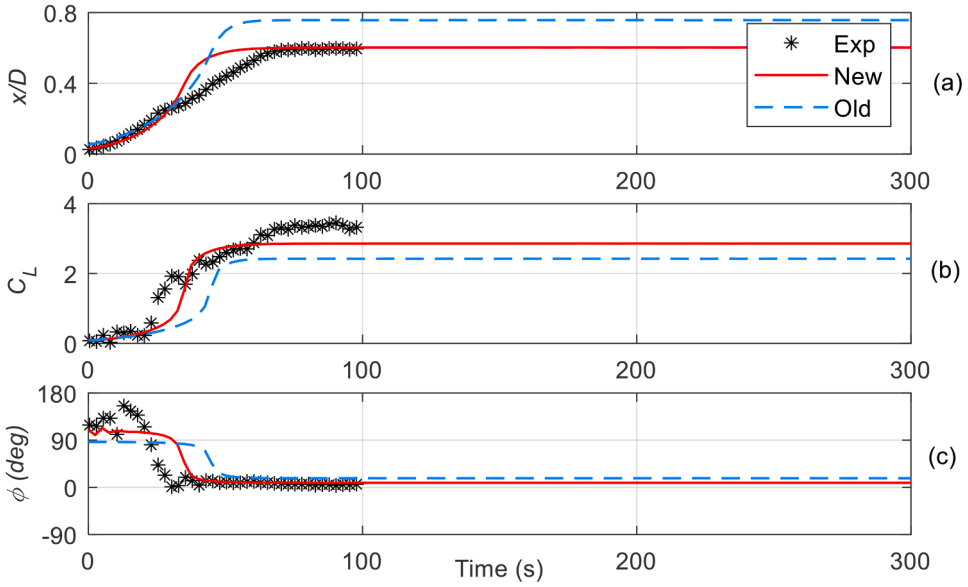

Fig. 15. Build-up test, numerical-experimental comparison: point D in Fig. 13 ($U = 3.94$ m/s, $U/U_{St} = 1.17$): (a) non-dimensional oscillation amplitude, (b) lift coefficient, (c) relative phase.

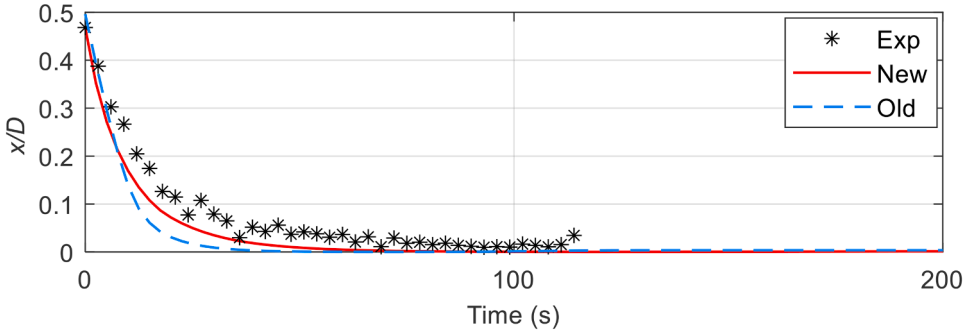

Fig. 16. Decay test, numerical-experimental comparison: point A in Fig. 13 ($U = 3.36$ m/s, $U/U_{St} = 0.91$).

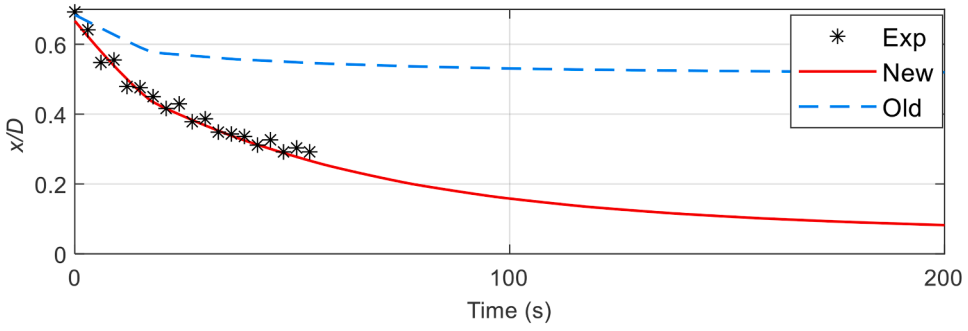

Fig. 17. Decay test, numerical-experimental comparison: point B in Fig. 13 ($U = 5.37$ m/s, $U/U_{St} = 1.45$).

5.1. Spectral analysis

The two build-up tests presented in the previous section were analysed also in terms of spectra comparing the time-frequency analysis of the lift force and the displacement obtained from experimental data and numerical ones (only new configuration is reported see Figs. 18 and 19).

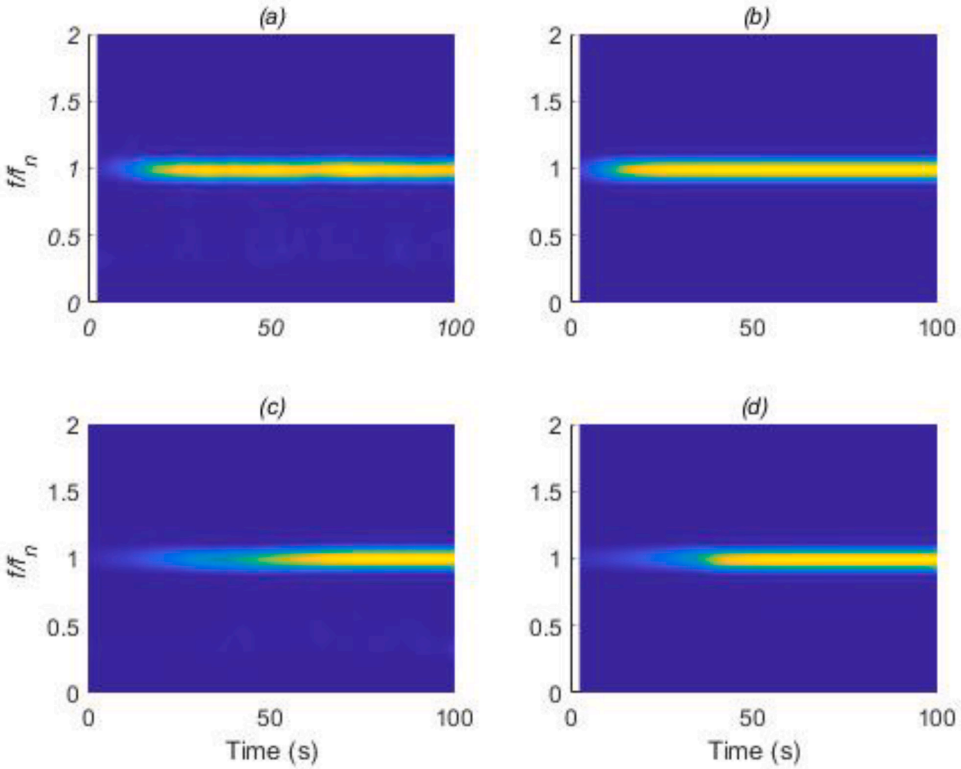

Fig. 18. Non-dimensional oscillation amplitude spectra as a function of the time and of the normalized frequency: numerical ((b) $U/U_{St} = 1.09$, (d) $U/U_{St} = 1.17$) and experimental ((a) $U/U_{St} = 1.09$, (c) $U/U_{St} = 1.17$) comparison for build-up tests.

It is confirmed that, also during the transient, the displacement signal is narrow band and monoharmonic, both in the experimental and the numerical case.

On the other hand, at the beginning of the time history, the lift force, in the experimental case, is characterized by the Strouhal frequency until synchronization becomes prevalent. This phenomenon is not present in the numerical signal, which shows only the cylinder motion frequency even for small oscillation amplitudes. This discrepancy was expected, but it was considered not relevant concerning the scope of the work.

5.2. Structural damping effects

The proposed research aimed to define a model that could be generalized to a cylindrical-shaped structure with different characteristics in terms of dimensions, Reynold numbers, natural frequencies, structural damping, etc. For this reason, the obtained model was tested against a different set of experimental data obtained using the same set-up previously described with increased structural damping (see Fig. 20). The results, presented in terms of steady-state response, are reported in Fig. 21 together with the old model curves. It is possible to note that the new model can reproduce only the first part of the lock-in region, underestimating its width. It represents, in any case, an improvement with respect to the old model, as its values are more in line with the experimental one especially as far as it concerns the oscillation amplitude the relative phase and the energy. Lower branch is anticipated and this can probably be due to a not accurate modeling of of the damping at oscillation amplitude higher than 0.5 diameter: the experimental data about structural damping are, in fact, available only up to this amplitude (see Fig. 20). A different fitting was used (see Fig. 22) and the results are reported in terms of oscillation amplitude in Fig. 23: it is possible to note that a slight improvement was achieved but the width of the lock-in region is still underestimated. Higher accuracy in the definition of the structural damping during experimental tests and a more refined model for the structural damping implementation in the numerical code would probably permit to achieve better results.

5.3. Comparison with literature data

In order to check the potential of the identified equivalent oscillator model, it was applied to a literature case included in Govardhan and Williamson [30]. In particular the high m^* case was considered as the equivalent oscillator was identified from experimental data characterized by high values of mass ratio. Moreover, as this model was developed mainly to be used for civil applications, its behavior in high m^*conditions was considered more relevant. The data presented in the reference paper refers to tests

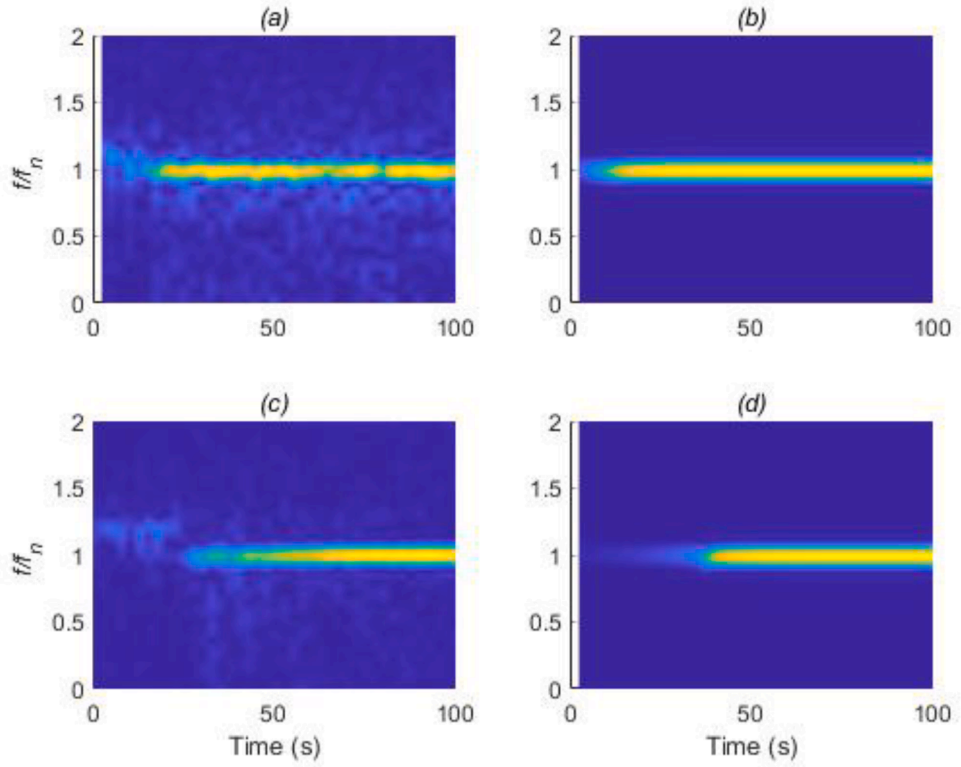

Fig. 19. Lift coefficient spectra as a function of the time and of the normalized frequency: numerical ((b) $\boldsymbol{U}/\boldsymbol{U}_{\boldsymbol{St}} = 1.09$, (d) $\boldsymbol{U}/\boldsymbol{U}_{\boldsymbol{St}} = 1.17$) and experimental ((a) $\boldsymbol{U}/\boldsymbol{U}_{\boldsymbol{St}} = 1.09$, (c) $\boldsymbol{U}/\boldsymbol{U}_{\boldsymbol{St}} = 1.17$) comparison for build-up tests.

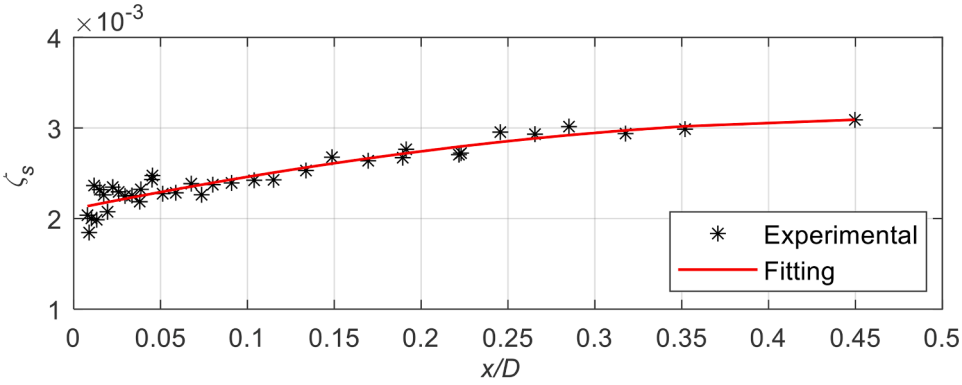

Fig. 20. Structural non-dimensional damping as a function of the oscillation amplitude, increased level.

performed in water, but for simplicity the simulations have been performed in air, adjusting the mass and the damping in order to obtain the same m^* and $m^*\zeta_s$. In Table 4 are summarized the main parameters considered for numerical model development and for the simulations.

In Fig. 24 the steady-state response in terms of non-dimensional oscillation amplitude obtained through the numerical simulations is compared with the literature data included in Govardhan and Williamson [30].

It is possible to note that, even if a not perfect match is obtained, the results can be considered satisfactory in consideration that this is a preliminary version of the equivalent oscillator model, and tuning and refinement can be performed in the future. In particular, the slope of the first branch is quite similar for the two curves and the maximum amplitudes reached are quite close to each other. The difference can be explained also considering that the literature data refers to lower *Re* Numbers (up to $4\ 10^3$) with respect to the ones of the data used for the identification procedure, and, as highlighted in Govardhan and Williamson [31], this can affect the maximum reached amplitude. The main differences concern the lower branch, but as explained in the previous chapters, this branch is less interesting for the considered applications of the model. Moreover, this result was expected considering the reduced lower branch of

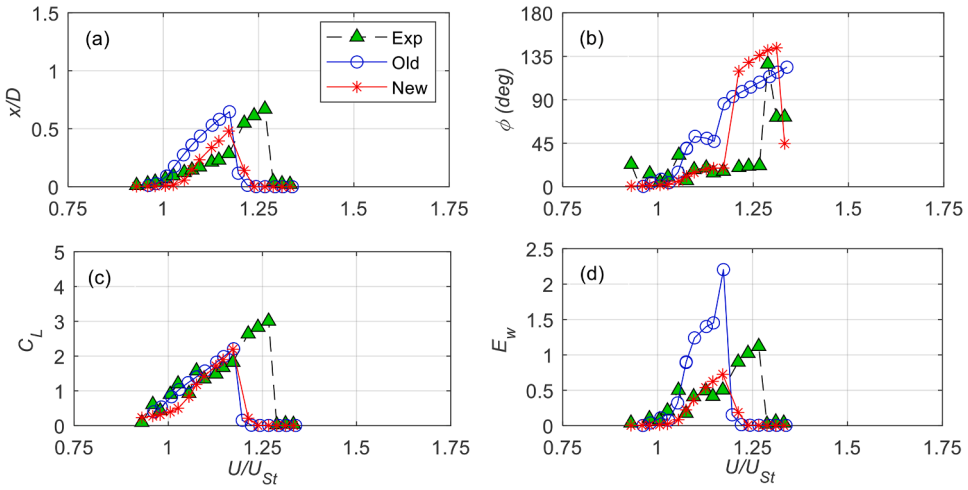

Fig. 21. Steady-state response of the oscillating cylinder in the lock-in region for a higher level of damping: (a) non-dimensional oscillation amplitude, (b) relative phase, (c) lift coefficient, (d) non-dimensional power input. Comparison between numerical (new and old) and experimental results.

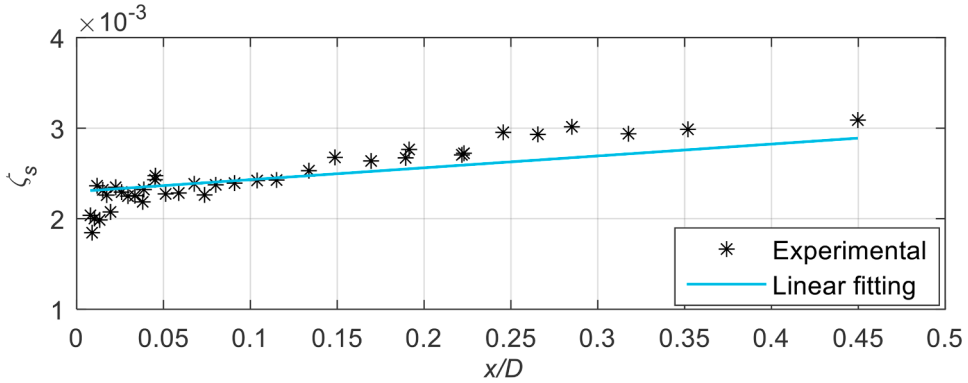

Fig. 22. Structural non-dimensional damping as a function of the oscillation amplitude, increased level and linear fitting.

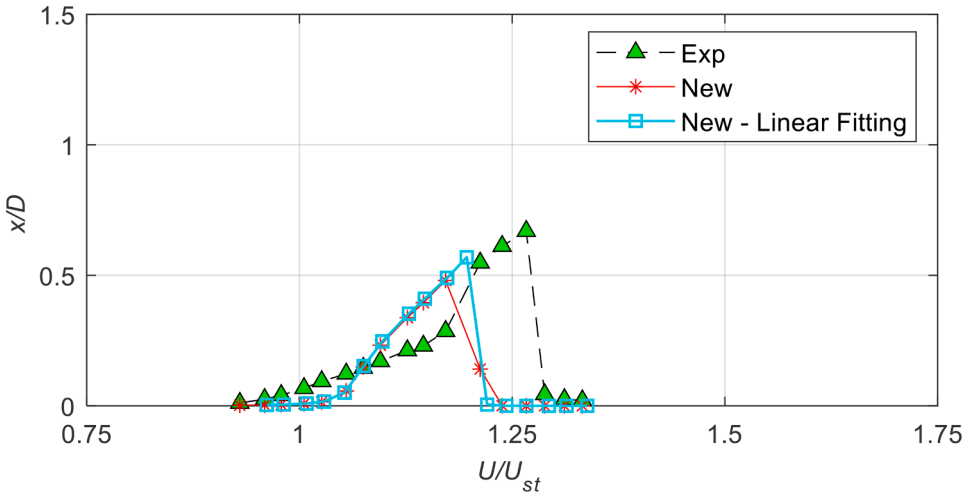

Fig. 23. Steady-state response of the oscillating cylinder in the lock-in region for a higher level of damping (non-dimensional oscillation amplitude): comparison between experimental and numerical results (two different damping fitting).

Table 4
Main model parameters for simulations reproducing the high m* case of Govardhan and Williamson [30].

Diameter D (m)	0.2
Length L (m)	2
Linear mass m/L (kg/m)	11.81
Natural frequency f_n (Hz)	3.1
Mass ratio m^*	320
Strouhal Number St	0.2
Reynolds Number Re (nominal value in lock-in region)	$5\ 10^4$
Non-dimensional damping ζ_s	$7.8\ 10^{-4}$
$m^*\ \zeta$	0.251

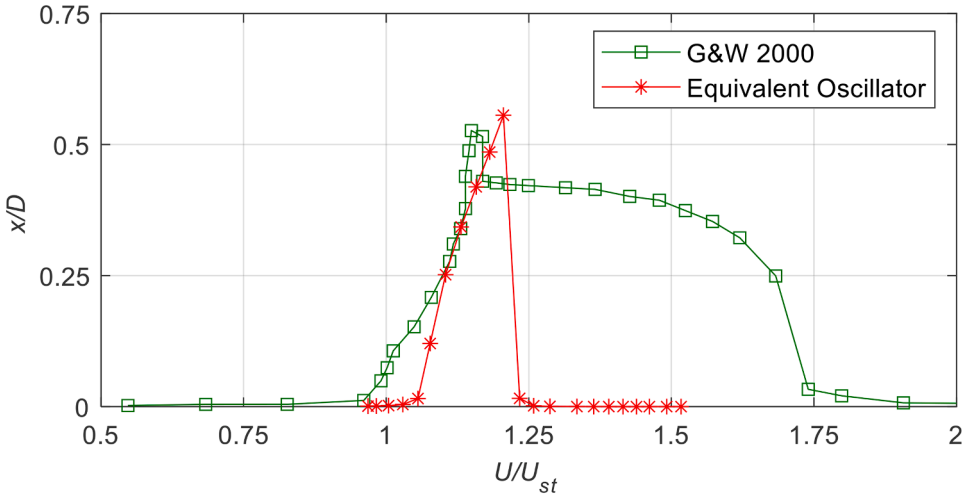

Fig. 24. Steady-state response in terms of non-dimensional oscillation amplitude for high m^* case of Govardhan and Williamson (2000): comparison between experimental data and the simulation results obtained applying the equivalent oscillator model.

the data used for the identification: by enlarging the identification database a better reproduction of this part of the curve could be obtained. These results confirm the possibility to use the same model for VIV in air and in water in high m^* conditions. In the case of low m^* the model would be still valid as long as the added mass effect is carefully considered and modeled.

6. Conclusions

VIV is an important phenomenon that affects bluff bodies and it can be relevant for several civil applications as cylindrical-shaped structures. In order to predict maximum reached amplitudes and eventually design a proper damping system, it is important to have numerical tools able to reproduce the main issues of the phenomenon avoiding large computational costs. Phenomenological models can be profitably used for these applications, in particular the Equivalent oscillator numerical model has been chosen referring to previous studies performed by Politecnico di Milano that highlighted its capability to reproduce the main requested VIV features. Starting from the past formulations, an update of the model was performed devoting particular attention to the definition of the characteristic parameters of the model, main responsible for its performances: for the identification procedure, a genetic algorithm based approach was used. Experimental data collected during a wide wind tunnel campaign on a cylinder rigid model elastically suspended were used partially as identification, and partially as validation database.

The obtained model can be considered satisfactory in matching the identified targets, in particular an improvement with respect to a previous version of the model has been obtained. The Equivalent oscillator model was then used to reproduce the high m^* case reported in Govardhan and Williamson [30]: a not perfect match was reached but the results are quite close to the literature data, especially for the most interesting part of the lock-in region. Further developments are still required to check the model capability to be generalized to a cylindrical-shaped structure with different characteristics in terms of dimensions, Reynold numbers, natural frequencies, structural damping. The application of the model along flexible structures to evaluate its capability in reproducing the behavior of the single section under wind profile conditions should also be tested. As the genetic algorithm based approach seems to be promising in identifying the model parameters, further checks and experimental tests are planned to enlarge the experimental database and refine the identification process.

CRediT authorship contribution statement

T. Argentini: Methodology, Writing – original draft, Supervision, Conceptualization. **S. Muggiasca:** Methodology, Writing – original draft, Supervision, Conceptualization. **G. Notaro:** Methodology, Validation, Formal analysis, Writing – original draft. **D. Rocchi:** Conceptualization, Writing – review & editing, Supervision. **F. Zanelli:** .

Declaration of competing interest

The authors declare that they have no known competing financial interests or personal relationships that could have appeared to influence the work reported in this paper.

The authors declare the following financial interests/personal relationships which may be considered as potential competing interests:

Data availability

Data will be made available on request.

References

[1] T. Sarpkaya, A critical review of the intrinsic nature of vortex-induced vibrations, J. Fluids Struct. 19 (2004) 389–447.
[2] C.H.K. Williamson, R. Govardhan, Vortex-induced vibrations, Annu. Rev. Fluid Mech. 36 (2004) 413–455.
[3] P. Bearman, Circular cylinder wakes and vortex-induced vibrations, J. Fluids Struct. 27 (2011) 648–658.
[4] C.H.K. Williamson, A. Roshko, Vortex formation in the wake of an oscillating cylinder, J. Fluids Struct. 2 (1988) 355–381.
[5] N. Jauvtis, C.H.K. Williamson, Vortex-induced vibration of a cylinder with two degrees of freedom, J. Fluids Struct. 17 (2003) 1035–1042.
[6] D. Brika, A. Laneville, Vortex-induced vibrations of a long flexible circular cylinder, J. Fluid Mech. 250 (1993) 481.
[7] A. Zasso, M. Belloli, S. Giappino, S. Muggiasca, Pressure field analysis on oscillating circular cylinder, J. Fluids Struct. 24 (2008) 628–650, https://doi.org/10.1016/j.jfluidstructs.2007.11.007.
[8] M. Belloli, S. Giappino, S. Muggiasca, A. Zasso, Force and wake analysis on a single circular cylinder subjected to vortex induced vibrations at high mass ratio and high Reynolds number, J. Wind Eng. Ind. Aerodyn. 103 (2012) 96–106, https://doi.org/10.1016/j.jweia.2012.03.005.
[9] S. Muggiasca, M. Belloli, G. Diana, Specific power input: comparison among rigid and flexible models, J. Wind Eng. Ind. Aerodyn. 173 (2018) 180–186, https://doi.org/10.1016/j.jweia.2017.12.004.
[10] Navrose, S. Mittal, Free vibrations of a cylinder: 3-D computations at *Re*=1000, J. Fluids Struct. 41 (2013) 109–118, https://doi.org/10.1016/j.jfluidstructs.2013.02.017.
[11] S. Mandelli, S. Muggiasca, S. Malavasi, Numerical simulation of an oscillating cylinder at high reynolds number, in: Proceedings of the International Conference on Offshore Mechanics and Arctic Engineering - OMAE, Nantes, France 7, 2013, V007T08A073, https://doi.org/10.1115/OMAE2013-11362 art.
[12] S. Mandelli, S. Muggiasca, S. Malavasi, Pressure field and wake modes analysis of an oscillating cylinder, Ocean Eng. 124 (2016) 74–83, https://doi.org/10.1016/j.oceaneng.2016.07.042.
[13] EN 1991-1-4: Eurocode 1: Actions on Structures - Part 1-4: General actions - Wind actions.
[14] R.E.D. Bishop, A.Y. Hassan, The lift and drag forces on a circular cylinder oscillating in a flowing fluid, Proceedings of the Royal Society of London. Series A. Mathematical and Physical Sciences 277 (1368) (1964) 51–75.
[15] R.T. Hartlen, I.G. Currie, Lift-Oscillator Model of Vortex- Induced Vibration, Journal of the Engineering Mechanics Division (1970), 1970.
[16] O.M. Griffin, R. A.Skop, G.H. Koopmann, The vortex-excited resonant vibrations of circular cylinders, J. Sound Vib. 31 (2) (1973) 235–249.
[17] R.D. Gabbai, H. Benaroya, An overview of modeling and experiments of vortex-induced vibration of circular cylinders, J. Sound Vib 282 (3–5) (2005) 575–616.
[18] M.L. Facchinetti, E. de Langre, F. Biolley, Coupling of structure and wake oscillators in vortex-induced vibrations, J. Fluids Struct. 2 (19) (2004) 123–140, https://doi.org/10.1016/j.jfluidstructs.2003.12.004.
[19] R.H.M. Ogink, A.V. Metrikine, A wake oscillator with frequency dependent coupling for the modeling of vortex-induced vibration, J. Sound Vib. 329 (26) (2010) 5452–5473, https://doi.org/10.1016/j.jsv.2010.07.008.
[20] M.A. Dhanwani, A. Sarkar, B.S.V. Patnaik, Lumped parameter models of vortex induced vibration with application to the design of aquatic energy harvester, J. Fluids Struct. 43 (2013) 302–324, https://doi.org/10.1016/j.jfluidstructs.2013.09.008.
[21] G. Diana, M. Gasparetto, Studio del fenomeno di distacco dei vortici da cilindri investiti da vena fluida mediante modello ad oscillatore equivalente (Study of the phenomenon of vortex detachment from cylinders invested by fluid vein using equivalent oscillator model), in: Congresso nazionale di Meccanica teorica e applicata, Firenze, 1978.
[22] M. Belloli, G. Diana, F. Resta, S. Muggiasca, A Numerical Model to Reproduce Vortex Induced Vibrations of a Circular Cylinder, American Society of Mechanical Engineers, Pressure Vessels and Piping Division (Publication) PVP, Vancouver, BC, Canada, 2006, p. 9, https://doi.org/10.1115/PVP2006-ICPVT-11-93972, 2006.
[23] T. Argentini, M. Belloli, F. Fossati, D. Rocchi, M. Villani, Experimental and numerical analysis of the dynamic response of cable-stayed bridge: vortex induced vibrations and buffeting effects, in: Conference: Proceedings of the 13th International conference on Wind Engineering, Amsterdam, 2011.
[24] M. Belloli, P. Borghesani, D. Rocchi, L. Rosa, M. Sbrosi, M. Villani, FRC erection stages dynamic behaviour under wind loads, in: Proceedings of the 8th International Conference on Structural Dynamics, EURODYN 2011, Leuven, Belgium, 2011, 4 - 6 July 2011.
[25] S. Muggiasca, S. Giappino, T. Argentini, A. Collina, A. Manenti, G. Diana, Wind Resistant Design of a Very Large Observation Wheel, Structural Engineering International (2021), https://doi.org/10.1080/10168664.2021.1911612.
[26] S.N. Sivanandam, S.N. Deepa, Introduction to Genetic Algorithms, Springer, 2008.
[27] J. Wróblewski, Theoretical Foundations of Order-Based Genetic Algorithms, Fundam Inform 28 (3,4) (1996) 423–430.
[28] A. Zasso, M. Belloli, S. Giappino, S. Muggiasca, On the Pressure and Force Field On a Circular Cylinder Oscillating in the lock- in region At Sub-Critical Reynolds number, American Society of Mechanical Engineers, Pressure Vessels and Piping Division (Publication) PVP, Vancouver, BC, Canada, 2006, pp. 919–927, https://doi.org/10.1115/PVP2006-ICPVT-11-93971, 9.
[29] M. Belloli, S. Giappino, S. Morganti, S. Muggiasca, A. Zasso, Vortex induced vibrations at high Reynolds numbers on circular cylinders, Ocean Eng. 94 (2015) 140–154, https://doi.org/10.1016/j.oceaneng.2014.11.017.
[30] C. Govardhan, C.H.K. Williamson, Modes of vortex formation and frequency response of a freely vibrating cylinder, J. Fluid Mech. 420 (2000) 85–130.
[31] C. Govardhan, C.H.K. Williamson, Defining the 'modified Griffin plot' in vortex-induced vibrations: revealing the effect of Reynolds number using controlled damping, J. Fluid Mech 560 (2006) 147–180.